



Insights into the Replisome from the Structure of a Ternary Complex of the DNA Polymerase III α -Subunit

Richard A. Wing^{1†}, Scott Bailey^{1,2†} and Thomas A. Steitz^{1,2,3*}

¹Department of Molecular Biophysics and Biochemistry, Yale University, New Haven, CT 06520, USA

²Howard Hughes Medical Institute, New Haven, CT 06510, USA

³Department of Chemistry, Yale University, New Haven, CT 06520, USA

Received 17 June 2008;

accepted 22 July 2008

Available online

27 July 2008

Edited by K. Morikawa

The crystal structure of the catalytic α -subunit of the DNA polymerase III (PolIII α) holoenzyme bound to primer-template DNA and an incoming deoxy-nucleoside 5'-triphosphate has been determined at 4.6-Å resolution. The polymerase interacts with the sugar-phosphate backbone of the DNA across its minor groove, which is made possible by significant movements of the thumb, finger, and β -binding domains relative to their orientations in the unliganded polymerase structure. Additionally, the DNA and incoming nucleotide are bound to the active site of PolIII α nearly identically as they are in their complex with DNA polymerase β , thereby proving that the eubacterial replicating polymerase, but not the eukaryotic replicating polymerase, is homologous to DNA polymerase β . Finally, superimposing a recent structure of the clamp bound to DNA on this PolIII α complex with DNA places a loop of the β -binding domain into the appropriate clamp cleft and supports a mechanism of polymerase switching.

© 2008 Elsevier Ltd. All rights reserved.

Keywords: eubacterial DNA replication; DNA polymerase III; OB-fold; ternary complex; nucleotidyltransferase

Introduction

The DNA polymerase III (PolIII) holoenzyme replicates the genome of eubacteria. This 15-subunit complex functions as a tripartite assembly consisting of the core polymerase, the clamp loader, and the clamp.¹ In *Escherichia coli*, the core polymerase contains the catalytic α -subunit (PolIII α), the 3'-5' exonuclease ϵ -subunit, and the θ -subunit, whose function is essentially unknown.² The ring-shaped clamp, which encircles duplex DNA,^{3,4} imparts processivity to the core polymerase through its interactions with PolIII α .⁵⁻⁷ The clamp loader operates as a heptameric adenosine 5'-triphosphate (ATP) hydrolase that loads the clamp onto RNA-primed sites prior to binding of clamp by DNA PolIII.⁸

DNA-dependent DNA polymerases have been classified into six families (A, B, C, D, X, and Y) based on analysis of their sequences.⁹⁻¹² Members of families A, B, C, and D participate directly in DNA replication. PolIII α , the main eubacterial replicating polymerase, is a C-family polymerase, whereas many archaeal and all eukaryotic replicative polymerases are B-family polymerases.⁹ X- and Y-family polymerases, such as the eukaryotic DNA polymerase β (Pol β) and the archaeal DNA polymerase IV (PolIV; Dpo4), respectively, are involved in DNA repair.^{9,10} Members of all six polymerase families accomplish polymerization utilizing three domains, termed the fingers, palm, and thumb.¹³ The fingers interact with the incoming nucleotide, the palm positions the catalytic Mg²⁺ ions that perform catalysis, and the thumb grips the DNA substrate, typically through backbone interactions with the minor groove.¹⁴ In addition to these domains, PolIII α also includes an N-terminal polymerase and histidinol phosphatase (PHP) domain,^{15,16} a β -binding domain that contains an "internal" clamp-binding site,^{17,18} and a C-terminal domain (CTD) that includes both an oligonucleotide-binding (OB) fold¹⁹ and an "external" clamp-binding site located at the extreme C-terminus of the polymerase.²⁰

The six polymerase families can be grouped into two superfamilies based on the fold of their palm domains. The palm domains of members of families

*Corresponding author. Department of Molecular Biophysics and Biochemistry, Yale University, New Haven, CT 06520, USA. E-mail address: thomas.steitz@yale.edu.

† R.A.W. and S.B. contributed equally to this work.

Abbreviations used: PolIII α , DNA polymerase III α -subunit; Pol β , DNA polymerase β ; PolIV, DNA polymerase IV; PHP, histidinol phosphatase; CTD, C-terminal domain; OB, oligonucleotide binding; β NT, Pol β -like nucleotidyltransferase; MR, molecular replacement; HhH, helix-hairpin-helix.

A, B, and Y are formed by a four-stranded antiparallel β -sheet,^{21–24} whereas members of families C and X have a palm domain formed by a five-stranded mixed β -sheet^{25–27} that belongs to the Pol β -like nucleotidyl-transferase (β NT) superfamily.²⁸ Although both types of palm domain folds utilize a two-metal-ion mechanism for catalysis, the two palm folds are considered to be cases of convergent evolution.²⁹ As such, this distinct difference between eukaryotic and eubacterial replicative polymerases may potentially be exploitable for the design of novel antibiotics.

A key difference between the conclusions concerning the functional implications of the two structures of unliganded PolIII α recently reported is whether the palm domain of PolIII α is homologous to the palm domain of Pol β and thus binds its DNA substrate and incoming deoxy-nucleoside 5'-triphosphate (dNTP) as Pol β does.^{25,27} Bailey *et al.*²⁵ determined the structure of the full-length protein from *Thermus aquaticus*, and Lamers *et al.*²⁷ determined that of a truncated mutant lacking the CTD from *E. coli* (throughout this article, *E. coli* and *T. aquaticus* residue numbers have the prefixes "Eco" and "Taq", respectively). Lamers *et al.* concluded that *E. coli* PolIII α is not homologous to Pol β and cannot bind DNA as Pol β does because when they homology modeled the DNA, by superimposing the structures of PolIII α and the ternary complex of Pol β using their catalytic aspartates and the β -sheets of their palms, the homology-modeled DNA directly clashed with a short α -helix (residues Eco543–Eco549 and Taq605–Taq612) adjacent to the active-site aspartates of the palm domain (the active-site helix). Therefore, to model a complex of *E. coli* PolIII α with DNA, the authors placed a segment of standard B-form DNA into the PolIII α active site and rotated its orientation so that it did not overlap significantly with the protein and such that it could also interact with the β -binding domain. Their resulting model places the plane of the base pairs of the active-site DNA in an orientation not parallel with the direction of the β -strands of the palm domain, whereas the hallmark of DNA binding in the X family is that the plane of the base pairs is parallel with the direction of the β -strands of the palm domain.^{30,31} In contrast, Bailey *et al.* concluded that the palm domains of PolIII α and Pol β are homologous and found that homology modeling the DNA from the ternary complex of Pol β onto the structure of *T. aquaticus* PolIII α resulted in no main-chain clash between the DNA and the palm domain, including the active-site helix. Consequently, they were able to produce a model of the DNA complex in which the plane of the base pairs is parallel with the direction of the β -strands, as is the case in the structure of the ternary complex of Pol β . In this model, the β -binding domain was also hypothesized to rotate toward and interact with the DNA duplex.

Clearly, at least one of these two models of the DNA complex as well as the associated conclusions had to be incorrect. The crystal structure of *T. aquaticus* PolIII α bound to primer-template DNA with incoming nucleotide presented here establishes that, in contrast

to the conclusion of Lamers *et al.*,²⁷ PolIII α does indeed bind DNA and incoming nucleotide as Pol β does. Consequently, PolIII α is homologous to Pol β and not to the replication DNA polymerases of eukaryotes.

Results

Mutagenesis and inactivation of the N-terminal PHP nuclease domain

The N-terminal PHP domain of *Thermus thermophilus* PolIII α possesses a novel Zn²⁺-dependent exonuclease activity,¹⁶ which had to be inactivated in order to co-crystallize a complex between *T. aquaticus* PolIII α and its DNA substrate. The crystal structure of the unliganded *T. aquaticus* PolIII α exhibited two Zn²⁺ ions bound in a deep cleft within the PHP nuclease domain.²⁵ Site-directed mutagenesis was employed to eliminate two of the observed side-chain ligands of the Zn²⁺ ions by mutating two aspartates (Taq20 and Taq212) to asparagines (Supplementary Fig. 1). The nuclease activity of this double mutant on a substrate of primer-template DNA was significantly attenuated when compared with wild-type protein of equivalent purity (Supplementary Fig. 2). However, the residual nuclease activity could be completely inhibited by the addition of 2',3'-dideoxycytidine-5'-triphosphate (ddCTP) and 2'-dATP to the reaction buffer. Under these conditions, the primer strand was terminated by the incorporation of 2',3'-dideoxycytidine-5'-monophosphate and, subsequently, the dATP bound stably to the incoming nucleotide site, which resulted in a stable ternary complex of polymerase, primer-template DNA, and incoming nucleotide. It is presumably the stability of this complex that restricts the PHP nuclease domain's access to the DNA, thereby further inhibiting the nuclease activity.

Structure determination

The ternary complex of the D20N/D212N double mutant of *T. aquaticus* PolIII α with the ddCTP-terminated primer-template DNA and dATP was crystallized. The structures of several other ternary complexes of DNA polymerases have been determined by employing an analogous strategy.^{31,32} The resulting crystals diffracted X-rays to beyond 4.9-Å resolution, where the I/σ is 2.0. Although these crystals were merohedrally twinned, as could be demonstrated by analyzing the distribution of diffraction intensities,³³ phases were readily obtained by molecular replacement (MR) using the unliganded structure of *T. aquaticus* PolIII α as a search model.²⁵ Two copies (A and B) of the polymerase ternary complex were found in the asymmetric unit. Given the resolution of the X-ray data, optimization of the model was restricted to rigid-body refinement of the positions of the individual domains (see Experimental Procedures) and the subsequent analysis of the interactions between the polymerase and

Table 1. Crystallographic data and refinement statistics of the ternary complex of PolIII α

Space group	$P4_1$
Unit cell dimensions (Å)	$149.546 \times 149.546 \times 163.338$
Resolution (Å)	50–4.6
No. of unique reflections	20,097
R_{sym} (%) ^{a,b}	7.8 (70.0)
I/σ ^a	15.3 (1.4)
Completeness (%) ^a	99.7 (97.6)
Redundancy ^a	3.6 (3.0)
Copies in the asymmetric unit (AU)	2
R_{cryst} (%) ^c	28.7 (37.4)
R_{free} (%) ^c	27.1 (36.7)
Twin fraction (%)	45
No. of protein atoms in AU	18,338
No. of DNA atoms in AU	1583
No. of dNTP atoms in AU	58
No. of metal atoms in AU	2
PDB ID	3E0D

^a Numbers in parentheses correspond to the highest-resolution shell.

^b $R_{\text{sym}} = \sum |I - \langle I \rangle| / \sum I$, where I is the observed intensity and $\langle I \rangle$ is the average intensity of multiple observations of symmetry-related reflections.

^c After rigid-body refinement.

its substrates was limited to whether alternate side-chain rotamers could bring the side chains into contact distance with the substrates. The final model was refined at 4.6-Å resolution, where the I/σ is 1.4. This resolution was chosen due to the low values of the twinned R -factor and R_{free} (36.9% and 37.6%, respectively) obtained in the high-resolution shell (Table 1). The ultimate testament to the accuracy of the model was seen when inspecting the twofold averaged electron density map calculated using

phases from the protein coordinates alone before the DNA and incoming dNTP were incorporated into the model (twinned R -factor and R_{free} values of 31.4% and 30.4%, respectively). Readily apparent in this unbiased electron density map were features corresponding to the major and minor grooves of the double-stranded primer–template DNA as well as the triphosphate moiety of the incoming dNTP (Fig. 1 and Supplementary Fig. 3). The two copies of the protein components of the ternary complex found in the asymmetric unit are essentially identical with an rmsd of 1.1 Å over 1148 C α atoms. The DNA substrates are effectively identical apart from a bend in the DNA after the –12-position in copy A that is imposed by crystal packing (Supplementary Fig. 4). However, after this position, there is no observed contact between the polymerase and the DNA in both copies. Furthermore, the positions of the incoming nucleotide and the 3' primer terminus are identical in both copies. We have chosen to discuss copy B here because its DNA substrate appears unperturbed by crystal packing. The final model including the DNA and incoming dNTP has twinned R -factor and R_{free} values of 28.7% and 27.1% (Fig. 2a), respectively. Data collection and refinement statistics are presented in Table 1.

The overall structure of PolIII α and substrate interactions

Upon binding the primer–template DNA, the finger, thumb, and β -binding domains of PolIII α are seen to move toward the DNA bound to the palm and grip its backbone at the minor groove (Supplemental Movie 1). The thumb domain uses several positively charged residues within two α -helices

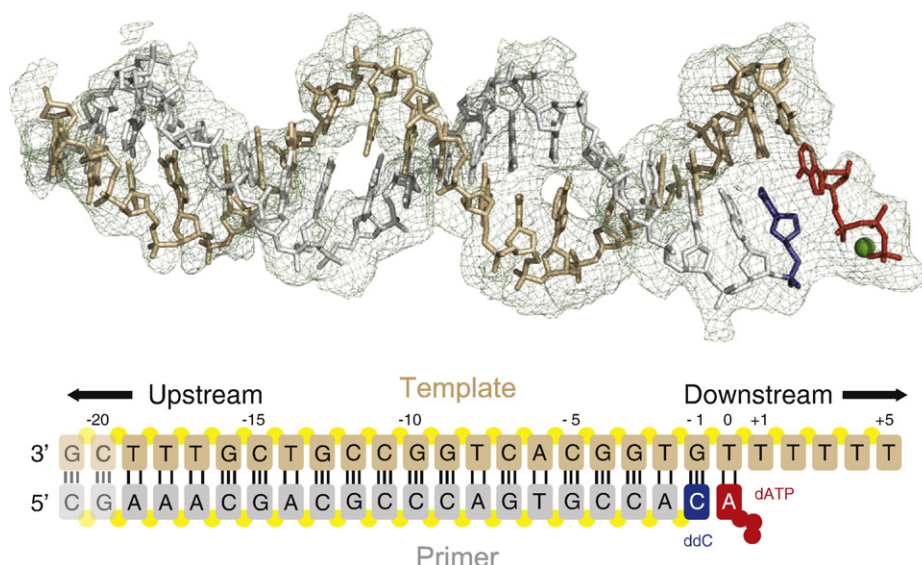


Fig. 1. DNA substrate density and schematic. Top: Electron density map calculated using observed amplitudes and phases calculated from the protein coordinates alone and contoured at 1σ . The observed DNA substrate is depicted using a stick representation. Bottom: The primer and template strands are shown in gray and wheat, respectively. The bases are represented as rounded rectangles with the phosphate backbone represented as yellow circles. The primer-terminal 3' ddC base is shown in blue, and the incoming nucleotide is shown in red. The numbering used to identify specific bases is indicated in black above the template strand. The two bases of the substrate that are not observed in the crystal structure at the –20- and –21-positions are rendered transparent.

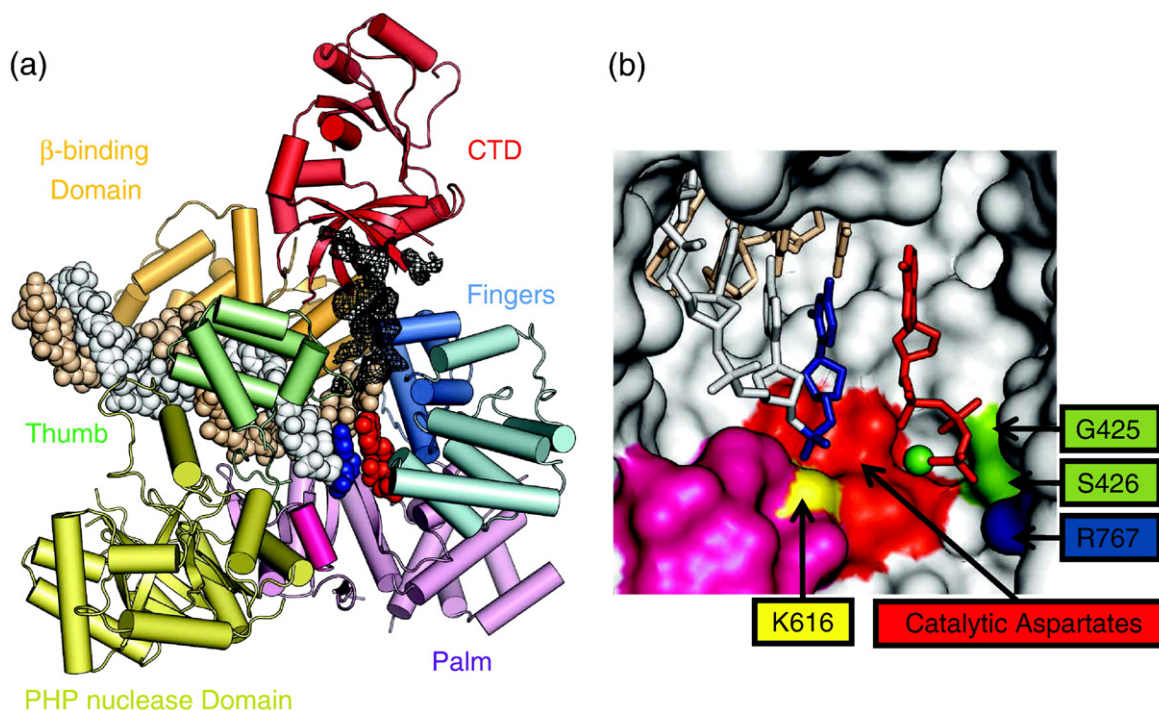


Fig. 2. Crystal structure of a replicating complex of *T. aquaticus* PolIII α . (a) A view of the crystal structure of the replicating complex of *T. aquaticus* PolIII α . Domains are labeled as follows: PHP nuclease, yellow; palm, pink; thumb, light green; index finger, light blue; middle finger, dark blue; β -binding, orange; and CTD, red. The template and primer strands are represented as spheres and shown in wheat and white, respectively. The primer-terminal 3' base is depicted with blue spheres, and the incoming nucleotide is depicted with red spheres. PolIII α is depicted in a cartoon representation. The density for the downstream DNA template strand is represented in mesh. (b) Close-up of the active site of PolIII α . PolIII α is depicted using a surface representation. The DNA substrate is depicted as sticks and shown as in the left panel. The incoming nucleotide and primer-terminal 3' base are shown in red and blue, respectively. Key active-site residues are labeled as follows: D463, D465, and D618 are shown in red; K616 is in yellow; S426 is in green; and R767 is in blue. The active-site helix is shown in magenta.

(residues Taq500–Taq511 and Taq515–Taq526) that lie parallel with the DNA helical axis and loops emanating from the palm domain to make electrostatic interactions with the sugar–phosphate backbone of the minor groove (Fig. 3a). A loop (Taq527–Taq535 and Eco465–Eco471) at the tip of the thumb extends toward the polymerase active site. More distant from the active site, the β -binding domain interacts with the DNA substrate using its helix–hairpin–helix (HhH) motif and flanking loops (Fig. 3b). The HhH motif presumably utilizes a bound metal ion to mediate interactions between the protein and the phosphates of the backbone, as is seen in the structures of other complexes of HhH motifs with DNA.³⁴ The two flanking loops appear to contact the sugar–phosphate backbone of the DNA directly using positively charged residues (Taq848, Taq932, Taq933, and Taq895). The finger domain completes the substrate-binding cleft by forming a wall toward which the 3' end of the primer is oriented. In addition, the finger domain acts in concert with the palm and the 3'-terminus of the primer to create a pocket that coordinates the incoming dATP molecule. The PHP nuclease domain does not contact the DNA substrate except possibly for a loop (residues Taq232–Taq241) situated below the thumb domain (Supplementary Fig. 5).

The 3' end of the primer strand and the incoming dNTP appear to be coordinated by several highly conserved residues in the active site (Fig. 2b). The phosphate group of the 3' primer terminus is positioned by electrostatic interactions with a lysine residue (Taq616) of the palm domain. Although at the current resolution the precise interactions are not clear, the binding pocket for the base and sugar moieties of the incoming dNTP appear to be primarily formed by residues from the finger domain (Taq698 and Taq813–821). However, clear electron density corresponding to the triphosphate moiety of the incoming dNTP (Fig. 1) is seen above the three aspartate residues (Taq463, Taq465, and Taq618) that have been previously seen by site-directed mutagenesis to be essential for catalysis.³⁵ The γ -phosphate of the incoming dNTP appears to contact the side chain of the serine of the glycine–serine (GS) motif (Taq425–Taq426), a motif found in all NTs,²⁸ as well as an arginine residue (Taq767) from the finger domain. All polymerases utilize a two-metal-ion mechanism of catalysis.²⁹ One metal ion (metal B) sits between the triphosphate moiety of the incoming nucleotide and the catalytic aspartates, while the second metal ion (metal A) is coordinated by the α -phosphate of the incoming nucleotide and the primer-terminal 3' hydroxyl. At the current resolu-

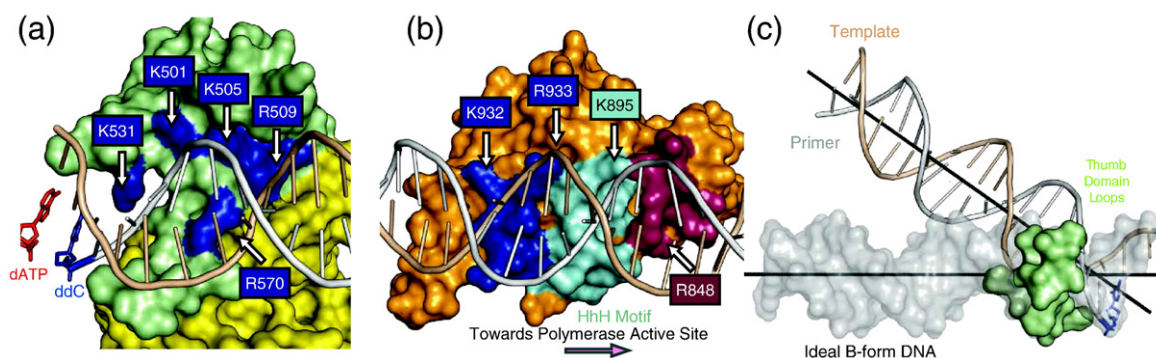


Fig. 3. Interactions with the DNA substrate. (a) Surface representation of interactions between the thumb domain of PolIII α and the DNA substrate in a cartoon representation. Green surfaces indicate the thumb domain, with blue surfaces representing residues proposed to interact with the DNA substrate. Yellow surfaces represent the PHP nuclease domain. The polymerase active site is seen on the left as demarcated by the blue stick representation of the primer-terminal 3' base (ddC) and the red stick representation of the incoming nucleotide (dATP). (b) Surface representation of interactions between the β -binding domain of PolIII α and the DNA substrate in a cartoon representation. Orange surfaces indicate the β -binding domain with three key loops implicated in DNA binding labeled as follows: Taq927–Taq923, blue; HhH motif Taq892–Taq910, cyan; and Taq846–Taq852, purple. Positively charged residues that are within proximity to interact with the sugar–phosphate backbone are labeled, and their positions are indicated with white arrows. An additional arrow points to the location of the polymerase active site. (c) The observed DNA substrate of PolIII α is depicted using a cartoon representation with the primer strand shown in white and the template strand shown in wheat. Idealized B-form DNA aligned with the DNA substrate prior to bending is displayed in a surface representation. Black lines indicate the helical axes of the DNA substrate (outside of the active site) and the idealized B-form DNA. The primer-terminal 3' base is represented in blue sticks. The loops of the thumb domain (Taq492–Taq499 and Taq569–Taq575) that induce DNA bending are shown in green and represented as a surface.

tion, it is difficult to assign the position of metal ions into our electron density maps. However, we assume that at a minimum, metal B has to be present in order to bridge the interaction between the negatively charged triphosphate moiety of the dNTP and the negative charge of the catalytic carboxylates. It is probable that any metal ions present at the polymerase active site are calcium ions rather than magnesium ions because the crystals were obtained in the presence of 10 mM magnesium chloride and 100 mM calcium chloride.

Conformation of the primer–template DNA

The electron density corresponding to the upstream duplex is consistent with the conformation of B-form DNA (Fig. 2a), as observed previously in the structures of the ternary complexes of Pol β ^{31,36} and RB69 polymerase.³⁷ However, a 30° bend, whose midpoint is located at the –2-position (Fig. 1), is imposed in the DNA by the loops that connect the thumb and palm domains (Fig. 3c). The current electron density maps are too ambiguous to model the base moieties of the downstream template; however, the path of the sugar–phosphate backbone is clear (Fig. 2a). The downstream template exits the active site with a sharp kink that is imposed by the finger domains, as has also been seen in other ternary complex structures.^{31,32,37–39} In contrast to other DNA polymerases, PolIII α appears to interact via the OB fold of its CTD more extensively with the downstream single-stranded DNA template (Fig. 2a), consistent with the suggested role of the CTD in the lagging-strand processivity switch.^{25,40}

Conformational changes induced by substrate binding

A comparison of the unliganded and ternary complex structures of *T. aquaticus* PolIII α reveals numerous conformational changes in the polymerase that take place upon binding DNA, some of which are similar to those that were previously predicted²⁵ and some of which were unanticipated but are functionally important. As predicted, the β -binding domain rotates by ~20° toward the palm, thereby allowing it to interact with the DNA substrate (Fig. 4a; Supplemental Movie 1) and positioning the internal clamp-binding site of the polymerase adjacent to the upstream duplex DNA (see below). The CTD rotates in conjunction with the β -binding domain but, as was not predicted, also undergoes an additional ~10° rotation that appears to bring its OB fold into a position to bind the downstream single-stranded DNA template strand (Fig. 4b; Supplemental Movie 2). Movement of the thumb away from the PHP domain (Fig. 4a) optimally positions the thumb to grip the duplex DNA from the –3-position to the –10-position (Fig. 3a). Only a minor displacement of the PHP nuclease domain is observed. A 15° rotation of a region within the finger domain (residues Taq699–Taq810), denoted as the index finger by Lamers *et al.*,²⁷ inward toward the palm (Fig. 4a) appears to help form the binding pocket for the bound incoming nucleotide. In particular, this movement positions an absolutely conserved arginine residue (Taq767) within contact distance of the γ -phosphate of the incoming nucleotide. A similar closing of the finger

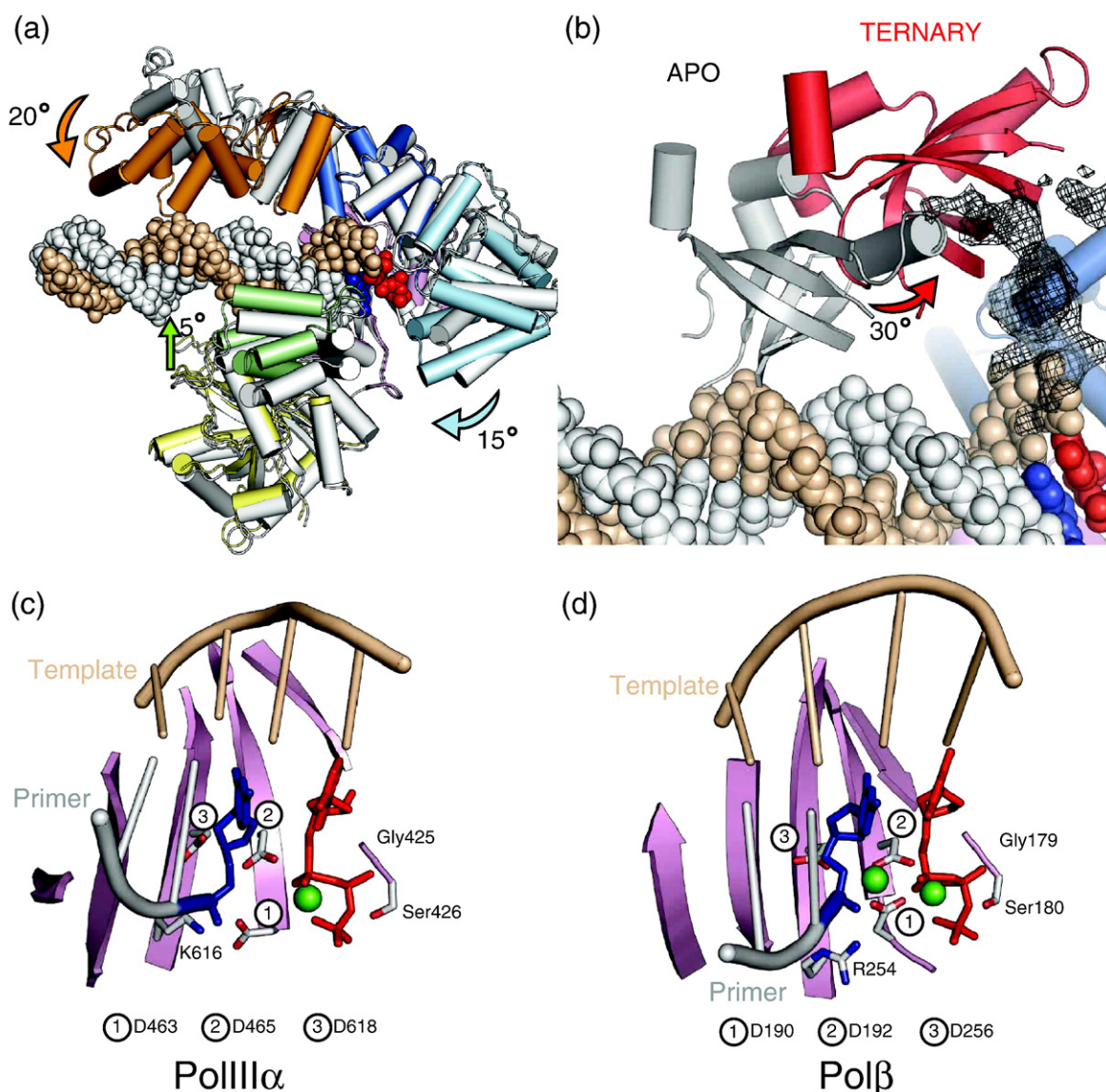


Fig. 4. Comparison of Pol β and PolIII α and conformational changes. (a) Cartoon depiction of domain changes in PolIII α associated with binding of DNA substrate. Domains are colored as in Fig. 2. Colored arrows indicate the direction of domain movement. Domain positions from the unliganded PolIII α structures are presented in a cartoon representation and shown in gray. (b) Changes in the position of the OB fold associated with binding of DNA substrate. The positions of the OB fold of PolIII α in unliganded and ternary complex conformations are presented in a cartoon representation and shown in gray and red, respectively. Here, the very C-terminus of the CTD and the β -binding domain are omitted for clarity. The density for the downstream DNA template strand is represented in mesh. (c) The polymerase active site in the structure of the ternary complex of PolIII α . The DNA substrate, the primer-terminal 3' base, and the incoming nucleotide are colored as in Fig. 2. The primer-terminal 3' base and incoming nucleotide are represented as sticks. The five β -sheets of the palm domain and the DNA substrates are displayed in a cartoon representation and shown in pink and wheat for the template and white for the primer. (d) The polymerase active site in the structure of the ternary complex of Pol β .

domain has been observed in the structures of other polymerase ternary complexes.^{32,37–39}

Discussion

PolIII α binds active-site DNA in the same manner as Pol β

Although the previously determined structures of the unliganded *E. coli* fragment of PolIII α ²⁷ and the

intact enzyme from *T. aquaticus* were interpreted differently with respect to whether PolIII α is homologous to Pol β and hence binds its DNA substrate similarly, the structure of the presented ternary complex of *T. aquaticus* PolIII α both resolves and explains these differences. The structures of the palm domains of PolIII α and Pol β are the same as noted by Bailey *et al.*;²⁵ additionally, the structures of the ternary complexes of PolIII α and Pol β show the same orientation of their DNA substrates relative to their palm domains. In both cases, the plane of the

base pairs of the DNA substrate is parallel with the strands of the palm domain. Furthermore, the positions of the active-site residues, 3' primer terminus, and incoming nucleotide are likewise similar. These elements are positioned nearly identically to accomplish catalysis in the ternary complex structures of PolIII α and Pol β (Fig. 4c and d). Once in the active site, two Mg²⁺ ions, the triphosphate moiety of the incoming nucleotide, and the primer-terminal 3' hydroxyl must be properly positioned in order for the phosphoryl transfer reaction to occur. The catalytic magnesium ions will be coordinated by three conserved aspartate residues (Taq463, Taq465, and Taq618). A conserved GS motif, two arginine residues (Taq452 and Taq458), and a magnesium ion (metal B) coordinate the triphosphate moiety of the incoming nucleotide. Positioning of the primer-terminal 3' hydroxyl relies on coordination of the primer-terminal phosphate by Taq616 and one of the two magnesium ions (metal A). Indeed, a least-squares superposition of the 3' primer terminus, the incoming nucleotide, the conserved Mg²⁺-binding catalytic aspartates, the GS motif, and the lysine (Taq616) observed in the structure of the ternary complex of PolIII α onto the equivalent residues of Pol β (D190, D192, D256, G179, S180, and R254) results in an rmsd of 1.36 Å over the C α atoms of the protein residues and all the atoms of the incoming nucleotide.

These similarities between the structures of the PolIII α and Pol β ternary complexes not only confirm that the palm domains share the same fold but also importantly establish that they bind DNA in the same manner, thereby providing further evidence that they share a common ancestor. It is not surprising, however, that the pathway of the DNA

outside the active site diverges between the two enzymes, since they do not share any common protein folds outside of the palm domain.

Comparison of the *E. coli* and *T. aquaticus* PolIII α structures

Comparison of the overall structures of unliganded *E. coli* PolIII α and the ternary complex of *T. aquaticus* PolIII α explains the different previous conclusions concerning the homology of PolIII α to Pol β and DNA binding. Although in the unliganded *E. coli* structure the β -binding domain and fingers are in a more open conformation and the thumb and PHP nuclease domains are rotated away from the palm domain, the movement of the thumb, finger, and β -binding domain that would be required for the *E. coli* PolIII α to form a ternary complex is consistent with the conformational changes that are observed between the structures of unliganded *T. aquaticus* PolIII α and its ternary complex. However, the critical difference between the *E. coli* and *T. aquaticus* PolIII α structures^{25,27} is the conformation of the β -sheet of the palm domain, particularly the sixth strand of their palm domains that contains the third catalytic carboxylate residue (Taq618 and Eco555) (Fig. 5a). The distance between the C α atoms of the second (Eco403) and third (Eco555) catalytic carboxylates in the structure of *E. coli* PolIII α is 7.6 Å, compared with the distance of 4.57 Å in the structure of *T. aquaticus* PolIII α (Fig. 5a). The average distance between these C α atoms among the 16 structures of enzymes that possess the NT fold is 5 Å, with a standard deviation of 0.7 Å (Supplementary Fig. 6). Indeed, a least-squares fit of the C α atoms of the three catalytic carboxylates of *E. coli*

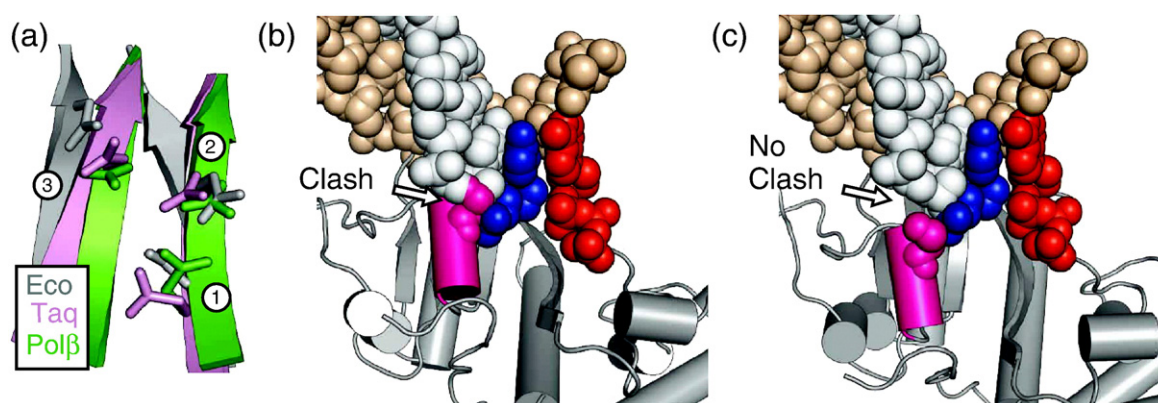


Fig. 5. Comparison of *E. coli* and *T. aquaticus* PolIII α structures. (a) The two sheets of the palm domain that contain the catalytic aspartate residues are depicted in a cartoon representation. The catalytic residues and sheets of the palm domains of *E. coli* PolIII α , *T. aquaticus* PolIII α , and Pol β are shown in gray, pink, and green, respectively. The catalytic aspartates are depicted as sticks and labeled as follows: "1" represents Eco401, Taq463, and D190 of Pol β ; "2" represents Eco403, Taq465, and D192 of Pol β ; and "3" represents Eco555, Taq618, and D256 of Pol β . (b) The palm domain of *E. coli* PolIII α in relation to the DNA substrate of *T. aquaticus* PolIII α when including the third catalytic carboxylate as a reference for superposition of the palm domain of *E. coli* PolIII α onto that of *T. aquaticus* PolIII α . The DNA substrate is depicted as in Fig. 1. The *E. coli* palm is shown in gray. The active-site helix is shown in magenta. A main-chain clash between the active-site helix of *E. coli* PolIII α and the DNA substrate of *T. aquaticus* PolIII α is indicated by a white arrow. Side chains closest to the DNA substrate are depicted as spheres. (c) A superposition of the palm domains of *E. coli* and *T. aquaticus* PolIII α when the third catalytic carboxylate is omitted as a reference.

PolIII α onto Pol β results in an rmsd of 1.8 Å *versus* that of 0.3 Å for the equivalent fit between *T. aquaticus* PolIII α and Pol β .

The conclusion of Lamers *et al.*²⁷ that “PolIII cannot bind DNA in a Pol β -like manner” resulted from the differences in the conformations of the structure of their palm domains, specifically the C-termini of their β -strands that contain the third catalytic carboxylate (Fig. 5a), complicating their ability to align the *E. coli* PolIII α structure with other structures containing the β NT fold. Lamers *et al.* included the third carboxylate in their alignment of the ternary complex of Pol β ³¹ onto their *E. coli* PolIII α structure, which resulted in main-chain clashes between the DNA substrate of Pol β and the active-site helix of *E. coli* PolIII α . Likewise, inclusion of the third catalytic carboxylate in an alignment of the palm domains of the structures of unliganded *E. coli* PolIII α and the ternary complex of *T. aquaticus* PolIII α results in similar clashes between the aligned DNA substrate of *T. aquaticus* PolIII α and the active-site helix of *E. coli* PolIII α (Fig. 5b). However, if superposition is performed by excluding the third catalytic carboxylate, then no clash is observed between the modeled DNA and the active-site helix of *E. coli* PolIII α (Fig. 5c). Main-chain clashes, however, are observed between the homology-modeled DNA and the C-terminus of the sixth strand that contains the third catalytic carboxylate. In

order to alleviate these clashes such that *E. coli* PolIII α can bind DNA in the same manner as *T. aquaticus* PolIII α and Pol β do, this strand must assume the same conformation that is observed in all other enzymes that utilize the β NT fold.

Thus, it appears that Lamers *et al.*²⁷ concluded that *E. coli* PolIII α does not bind DNA as Pol β does, because for some reason the tertiary structure of its palm domain is distorted. It is very unusual to find the ternary structure of a domain distorted, but it may be a result of crystal packing, removal of the CTD, or the lack of bound DNA. We expect that when the structure of a complex of *E. coli* PolIII α with DNA and dNTP is determined, this distorted palm domain conformation will change to that observed, and the resulting complex structure will closely resemble the structures of *T. aquaticus* PolIII α and Pol β .

A structural model of the complex between PolIII α , the clamp, and DNA

PolIII α accomplishes processive replication by partnering with the β -sliding clamp protein.^{7,41,42} In the absence of the clamp, the polymerase only replicates 10–20 nucleotides before falling off of the DNA substrate.^{41,43} Upon binding of the clamp, this processivity is increased to thousands of nucleotides

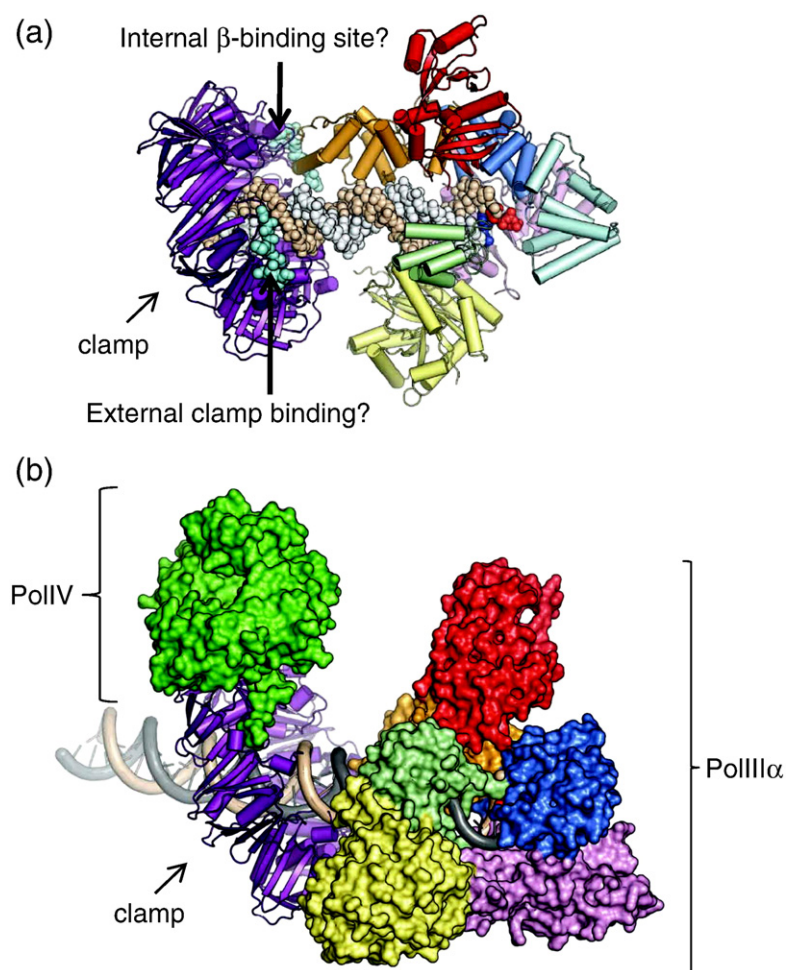


Fig. 6. Models of clamp binding to PolIII α and polymerase switching. (a) The polymerase and duplex DNA substrates are represented and colored as in Fig. 1. The clamp is presented in a cartoon representation and shown in purple. The polymerase-binding sites on the clamp are shown in cyan and depicted in a sphere representation. (b) Here, the model of two polymerases simultaneously bound to the sliding clamp is depicted with PolIII and PolIV in surface representation; colored as in Fig. 2 and in green, respectively; and rotated about the helical axis of the DNA into the page by about 60°. The clamp is depicted in a cartoon representation and shown in purple. The position of PolIV was achieved using a model of the little finger domain of *E. coli* PolIV bound to clamp (PDB ID 1UNN)⁴⁵ and the structure of the ternary complex of PolIV (PDB ID 1JXL)²¹ and the same modeling procedure as described by Indiani *et al.*⁴⁶

per binding event.^{7,41,42} The clamp is a dimeric protein that forms a ring-shaped molecule that contains two well-studied binding sites for polymerase on its N-terminal face.^{18,20}

The recent crystal structure of the β -sliding clamp bound to DNA³ allows us to construct a model of the interaction between PolIII α and clamp bound to primer-template DNA by superimposing the DNAs in the two co-crystal structures. Initially, the structure of the last base pair of the duplex DNA emanating from the N-terminal face of the clamp was superimposed on the structure of the last base pair of the upstream duplex DNA of the polymerase ternary complex, and then the structure of clamp and DNA was moved 1 bp at a time toward the polymerase until one of the two polymerase-binding sites [using Protein Data Bank (PDB) entry 1JQL from Jeruzalmi *et al.*⁴⁴] on the N-terminal surface of the clamp aligned with the internal clamp-binding site of the polymerase. The DNA was allowed to bend $\sim 5^\circ$ (Supplementary Fig. 7) to optimize the fit between the two proteins. Such a bend appears to be reasonable given that the DNA substrate is flexible past the -12 -position as observed in copy A of the polymerase ternary complex (Supplementary Fig. 4). The resulting model (Fig. 6a) produced no steric clash between the two proteins. Further movement of the clamp toward the polymerase by just 1 bp results in clashes between the clamp and the PHP domain as well as the β -binding domain of the polymerase, and movement of the clamp away from the polymerase by 1 bp rotates the polymerase-binding site of the clamp by 36° and out of contact distance with the polymerase. A striking finding in the clamp co-crystal structure with DNA is the 22° tilt of the clamp plane from being perpendicular to the DNA and its specific interactions with the DNA backbone. The excellent docking of the two complexes supports the validity of both the clamp-DNA interaction and the polymerase-DNA interaction. Additionally, the modeled distance of ~ 20 bp between the N-terminal surface of the clamp and $3'$ -terminus of the primer (Fig. 6a) is consistent with previous fluorescence,⁴⁷ cross-linking,⁴⁸ and DNA footprinting⁴⁹ experiments.

The clamp is a homodimer and thus has two identical protein-binding sites. Indeed, with the use of fluorescence energy transfer experiments, it has been shown that both PolIII and PolIV are able to bind clamp simultaneously.⁴⁶ It is believed that on encountering DNA damage, PolIII is displaced from the primer-template by PolIV and that, once PolIV has replicated past the damage, PolIII regains control of the primer-template DNA.⁴⁶ The tilted configuration of the DNA observed in the clamp-DNA structure may aid in this polymerase-switching mechanism.³ We have been able to dock the structure of PolIV onto our model of the structure of the complex between PolIII α , clamp, and DNA by superimposing the structure of full-length PolIV²¹ onto the structure of the clamp bound to the little finger domain of PolIV.⁴⁵ Consequently, these three co-crystal structures have allowed us to construct a model (Fig. 6b) of a complex between PolIII α , PolIV, clamp, and DNA that supports

the proposed mechanism of polymerase switching at points of DNA damage.^{3,46}

Experimental Procedures

Mutagenesis and protein purification

The exonuclease-deficient D20N/D212N double mutant of *T. aquaticus* PolIII α was generated using the Quik-Change method (Qiagen). The expression and purification of the mutant polymerase were performed as previously described for the wild-type protein,²⁵ except for a reduction from 200 to 50 mM in the concentration of sodium chloride in the gel filtration buffer.

Nuclease assays

The double mutant of *T. aquaticus* PolIII α (70 μ M) was incubated with primer-template DNA (140 μ M) either alone or in the presence of ddCTP (1 mM) and dATP (1 mM) at 37°C for 1 h or overnight. Reactions were quenched using a mixture of formamide and bromophenol blue and xylene cyanol dyes at a ratio of 4 volumes of dye mixture to 1 volume of reaction mixture. Subsequent to quenching, reactions were incubated at 90°C for 10 min prior to gel loading. Nuclease reactions were then loaded onto 25% acrylamide and 7 M urea denaturing gels run in Tris-borate-ethylenediaminetetraacetic acid buffer. The gel was stained with ethidium bromide for visualization.

Formation of the ternary complex

Ternary complex was formed by incubating D20N/D212N mutant polymerase (70 μ M) with MgCl_2 (10 mM), ddCTP (1 mM), dATP (1 mM), and primer-template DNA (primer sequence CGAAACGACGGCCAGTGCCA; template sequence TTTTGTGGCACTGGCCGTCGTT TCG) (140 μ M) for 1 h at 37°C .

Crystallization and data collection

Crystals were grown by the sitting-drop method of vapor diffusion, using well solutions consisting of 16%–21% (w/v) polyethylene glycol 400, 100 mM calcium chloride, and 100 mM Hepes, pH 6.9–7.2. Prior to flash freezing in liquid propane, crystals were transferred stepwise into a solution of 35% polyethylene glycol 400, 100 mM calcium chloride, and 100 mM Hepes, pH 6.9. Data were collected at beamline X-29 at the National Synchrotron Light Source of Brookhaven National Laboratory or at beamline 24-ID at the Advanced Photon Source. Data were integrated and scaled to 4.6 \AA (to an $\langle I \rangle / \sigma I$ of 1.4) using the HKL suite of programs.⁵⁰ Merohedral twinning of the crystals was detected in the program TRUNCATE,⁵¹ and the initial estimate of the twin fraction was determined in the Crystallography & NMR System.⁵² Crystallographic statistics are shown in Table 1.

Structure determination and refinement

In principle, crystal twinning should not hinder structure determination by MR.³³ Therefore, MR was performed with the twinned data in the program PHASER⁵³ using the unliganded *T. aquaticus* PolIII α structure²⁵ as a search model. Two copies of the polymerase were found

using this procedure, which were then broken into rigid bodies (body 1, residues 1–285; body 2, residues 286–492 and residues 576–522; body 3, residues 493–575; body 4, residues 523–835; body 5, residues 836–1012; and body 6; residues 1013–1220), and the positions of these rigid bodies were refined against the twinned amplitudes in the Crystallography & NMR System,⁵² including the twinning operator ($k, h, -l$), the twin fraction, and noncrystallographic symmetry restraints. Test reflections were selected such that all the twin-related pairs belonged to either the test set or the working set. The initial model output by PHASER yielded twinned R -factor and R_{free} values of 32.47% and 31.94%, respectively. Phases derived from this model were then improved by solvent flattening and twofold noncrystallographic symmetry averaging in the program DM⁵¹ using amplitudes that had been de-twinning by the program DETWIN.⁵¹ Individual rigid bodies were then fit to omit maps that, to further reduce model bias, were generated using phases that had been solvent flattened and twofold averaged. All of the model building was performed in the program Coot.⁵⁴ Omit maps of each of the polymerase domains can be seen in Supplementary Fig. 8. Once refinement and model building of the protein had converged, the DNA and incoming nucleotide were fit to their unbiased electron density (Fig. 1). The resulting ternary complex model was then subjected to a final round of rigid-body refinement. The final twin fraction of 45% was determined by comparing R_{free} values after refinement.

Accession numbers

The coordinates and structure factor amplitudes of the *T. aquaticus* PolIII α ternary complex have been deposited under the accession code 3E0D.

Acknowledgements

This research was supported by the National Institutes of Health through grant GM57510 to T.A.S. It was also supported by the National Institute of General Medical Sciences through grant T32GM007223 to R.A.W. The content is solely the responsibility of the authors and does not necessarily represent the official views of the National Institutes of Health or the National Institute of General Medical Sciences. We thank the staff at National Synchrotron Light Source beamline X-29 and Advanced Photon Source beamline 24-ID for helping with data collection.

Supplementary Data

Supplementary data associated with this article can be found, in the online version, at [doi:10.1016/j.jmb.2008.07.058](https://doi.org/10.1016/j.jmb.2008.07.058)

References

1. Kornberg, A. & Baker, T. (1992). *DNA Replication*. Freeman, New York, NY.

2. Johnson, A. & O'Donnell, M. (2005). Cellular DNA replicases: components and dynamics at the replication fork. *Annu. Rev. Biochem.* **74**, 283–315.
3. Georgescu, R. E., Kim, S. S., Yurieva, O., Kuriyan, J., Kong, X. P. & O'Donnell, M. (2008). Structure of a sliding clamp on DNA. *Cell*, **132**, 43–54.
4. Kong, X. P., Onrust, R., O'Donnell, M. & Kuriyan, J. (1992). Three-dimensional structure of the beta subunit of *E. coli* DNA polymerase III holoenzyme: a sliding DNA clamp. *Cell*, **69**, 425–437.
5. Kuwabara, N. & Uchida, H. (1981). Functional cooperation of the *dnaE* and *dnaN* gene products in *Escherichia coli*. *Proc. Natl Acad. Sci. USA*, **78**, 5764–5767.
6. LaDuca, R. J., Crute, J. J., McHenry, C. S. & Bambara, R. A. (1986). The beta subunit of the *Escherichia coli* DNA polymerase III holoenzyme interacts functionally with the catalytic core in the absence of other subunits. *J. Biol. Chem.* **261**, 7550–7557.
7. Stukenberg, P. T., Studwell-Vaughan, P. S. & O'Donnell, M. (1991). Mechanism of the sliding beta-clamp of DNA polymerase III holoenzyme. *J. Biol. Chem.* **266**, 11328–11334.
8. O'Donnell, M., Jeruzalmi, D. & Kuriyan, J. (2001). Clamp loader structure predicts the architecture of DNA polymerase III holoenzyme and RFC. *Curr. Biol.* **11**, R935–R946.
9. Filee, J., Forterre, P., Sen-Lin, T. & Laurent, J. (2002). Evolution of DNA polymerase families: evidences for multiple gene exchange between cellular and viral proteins. *J. Mol. Evol.* **54**, 763–773.
10. Ito, J. & Braithwaite, D. K. (1991). Compilation and alignment of DNA polymerase sequences. *Nucleic Acids Res.* **19**, 4045–4057.
11. Ohmori, H., Friedberg, E. C., Fuchs, R. P., Goodman, M. F., Hanaoka, F., Hinkle, D. *et al.* (2001). The Y-family of DNA polymerases. *Mol. Cell*, **8**, 7–8.
12. Patel, P. H. & Loeb, L. A. (2001). Getting a grip on how DNA polymerases function. *Nat. Struct. Biol.* **8**, 656–659.
13. Kohlstaedt, L. A., Wang, J., Friedman, J. M., Rice, P. A. & Steitz, T. A. (1992). Crystal structure at 3.5 Å resolution of HIV-1 reverse transcriptase complexed with an inhibitor. *Science*, **256**, 1783–1790.
14. Steitz, T. A. (1999). DNA polymerases: structural diversity and common mechanisms. *J. Biol. Chem.* **274**, 17395–17398.
15. Aravind, L. & Koonin, E. V. (1998). Phosphoesterase domains associated with DNA polymerases of diverse origins. *Nucleic Acids Res.* **26**, 3746–3752.
16. Stano, N. M., Chen, J. & McHenry, C. S. (2006). A coproofreading Zn(2+)-dependent exonuclease within a bacterial replicase. *Nat. Struct. Mol. Biol.* **13**, 458–459.
17. Dalrymple, B. P., Kongsuwan, K., Wijffels, G., Dixon, N. E. & Jennings, P. A. (2001). A universal protein–protein interaction motif in the eubacterial DNA replication and repair systems. *Proc. Natl Acad. Sci. USA*, **98**, 11627–11632.
18. Dohrmann, P. R. & McHenry, C. S. (2005). A bipartite polymerase–processivity factor interaction: only the internal beta binding site of the alpha subunit is required for processive replication by the DNA polymerase III holoenzyme. *J. Mol. Biol.* **350**, 228–239.
19. Murzin, A. G. (1993). OB(oligonucleotide/oligosaccharide binding)-fold: common structural and functional solution for non-homologous sequences. *EMBO J.* **12**, 861–867.
20. Lopez de Saro, F. J., Georgescu, R. E. & O'Donnell, M. (2003). A peptide switch regulates DNA polymerase processivity. *Proc. Natl Acad. Sci. USA*, **100**, 14689–14694.

21. Ling, H., Boudsocq, F., Woodgate, R. & Yang, W. (2001). Crystal structure of a Y-family DNA polymerase in action: a mechanism for error-prone and lesion-bypass replication. *Cell*, **107**, 91–102.
22. Ollis, D. L., Brick, P., Hamlin, R., Xuong, N. G. & Steitz, T. A. (1985). Structure of large fragment of *Escherichia coli* DNA polymerase I complexed with dTMP. *Nature*, **313**, 762–766.
23. Wang, J., Sattar, A. K., Wang, C. C., Karam, J. D., Konigsberg, W. H. & Steitz, T. A. (1997). Crystal structure of a pol alpha family replication DNA polymerase from bacteriophage RB69. *Cell*, **89**, 1087–1099.
24. Zhou, B. L., Pata, J. D. & Steitz, T. A. (2001). Crystal structure of a DinB lesion bypass DNA polymerase catalytic fragment reveals a classic polymerase catalytic domain. *Mol. Cell*, **8**, 427–437.
25. Bailey, S., Wing, R. A. & Steitz, T. A. (2006). The structure of *T. aquaticus* DNA polymerase III is distinct from eukaryotic replicative DNA polymerases. *Cell*, **126**, 893–904.
26. Davies, J. F., 2nd, Almassy, R. J., Hostomska, Z., Ferre, R. A. & Hostomsky, Z. (1994). 2.3 Å crystal structure of the catalytic domain of DNA polymerase beta. *Cell*, **76**, 1123–1133.
27. Lamers, M. H., Georgescu, R. E., Lee, S. G., O'Donnell, M. & Kuriyan, J. (2006). Crystal structure of the catalytic alpha subunit of *E. coli* replicative DNA polymerase III. *Cell*, **126**, 881–892.
28. Aravind, L. & Koonin, E. V. (1999). DNA polymerase beta-like nucleotidyltransferase superfamily: identification of three new families, classification and evolutionary history. *Nucleic Acids Res.* **27**, 1609–1618.
29. Steitz, T. A., Smerdon, S. J., Jager, J. & Joyce, C. M. (1994). A unified polymerase mechanism for nonhomologous DNA and RNA polymerases. *Science*, **266**, 2022–2025.
30. Garcia-Diaz, M., Bebenek, K., Krahn, J. M., Kunkel, T. A. & Pedersen, L. C. (2005). A closed conformation for the Pol lambda catalytic cycle. *Nat. Struct. Mol. Biol.* **12**, 97–98.
31. Pelletier, H., Sawaya, M. R., Kumar, A., Wilson, S. H. & Kraut, J. (1994). Structures of ternary complexes of rat DNA polymerase beta, a DNA template-primer, and ddCTP. *Science*, **264**, 1891–1903.
32. Doublié, S., Tabor, S., Long, A. M., Richardson, C. C. & Ellenberger, T. (1998). Crystal structure of a bacteriophage T7 DNA replication complex at 2.2 Å resolution. *Nature*, **391**, 251–258.
33. Yeates, T. O. (1997). Detecting and overcoming crystal twinning. *Methods Enzymol.* **276**, 344–358.
34. Doherty, A. J., Serpell, L. C. & Ponting, C. P. (1996). The helix-hairpin-helix DNA-binding motif: a structural basis for non-sequence-specific recognition of DNA. *Nucleic Acids Res.* **24**, 2488–2497.
35. Pritchard, A. E. & McHenry, C. S. (1999). Identification of the acidic residues in the active site of DNA polymerase III. *J. Mol. Biol.* **285**, 1067–1080.
36. Sawaya, M. R., Prasad, R., Wilson, S. H., Kraut, J. & Pelletier, H. (1997). Crystal structures of human DNA polymerase beta complexed with gapped and nicked DNA: evidence for an induced fit mechanism. *Biochemistry*, **36**, 11205–11215.
37. Franklin, M. C., Wang, J. & Steitz, T. A. (2001). Structure of the replicating complex of a pol alpha family DNA polymerase. *Cell*, **105**, 657–667.
38. Huang, H., Chopra, R., Verdine, G. L. & Harrison, S. C. (1998). Structure of a covalently trapped catalytic complex of HIV-1 reverse transcriptase: implications for drug resistance. *Science*, **282**, 1669–1675.
39. Li, Y., Korolev, S. & Waksman, G. (1998). Crystal structures of open and closed forms of binary and ternary complexes of the large fragment of *Thermus aquaticus* DNA polymerase I: structural basis for nucleotide incorporation. *EMBO J.* **17**, 7514–7525.
40. Leu, F. P., Georgescu, R. & O'Donnell, M. (2003). Mechanism of the *E. coli* tau processivity switch during lagging-strand synthesis. *Mol. Cell*, **11**, 315–327.
41. Bloom, L. B., Chen, X., Fyngenson, D. K., Turner, J., O'Donnell, M. & Goodman, M. F. (1997). Fidelity of *Escherichia coli* DNA polymerase III holoenzyme. The effects of beta, gamma complex processivity proteins and epsilon proofreading exonuclease on nucleotide misincorporation efficiencies. *J. Biol. Chem.* **272**, 27919–27930.
42. Maki, S. & Kornberg, A. (1988). DNA polymerase III holoenzyme of *Escherichia coli*: III. Distinctive processive polymerases reconstituted from purified subunits. *J. Biol. Chem.* **263**, 6561–6569.
43. Fay, P. J., Johanson, K. O., McHenry, C. S. & Bambara, R. A. (1981). Size classes of products synthesized processively by DNA polymerase III and DNA polymerase III holoenzyme of *Escherichia coli*. *J. Biol. Chem.* **256**, 976–983.
44. Jeruzalmi, D., Yurieva, O., Zhao, Y., Young, M., Stewart, J., Hingorani, M. *et al.* (2001). Mechanism of processivity clamp opening by the delta subunit wrench of the clamp loader complex of *E. coli* DNA polymerase III. *Cell*, **106**, 417–428.
45. Bunting, K. A., Roe, S. M. & Pearl, L. H. (2003). Structural basis for recruitment of translesion DNA polymerase Pol IV/DinB to the beta-clamp. *EMBO J.* **22**, 5883–5892.
46. Indiani, C., McInerney, P., Georgescu, R., Goodman, M. F. & O'Donnell, M. (2005). A sliding-clamp toolbelt binds high- and low-fidelity DNA polymerases simultaneously. *Mol. Cell*, **19**, 805–815.
47. Griep, M. A. & McHenry, C. S. (1992). Fluorescence energy transfer between the primer and the beta subunit of the DNA polymerase III holoenzyme. *J. Biol. Chem.* **267**, 3052–3059.
48. Reems, J. A., Wood, S. & McHenry, C. S. (1995). *Escherichia coli* DNA polymerase III holoenzyme subunits alpha, beta, and gamma directly contact the primer-template. *J. Biol. Chem.* **270**, 5606–5613.
49. Reems, J. A. & McHenry, C. S. (1994). *Escherichia coli* DNA polymerase III holoenzyme footprints three helical turns of its primer. *J. Biol. Chem.* **269**, 33091–33096.
50. Otwinowski, Z. & Minor, W. (1997). Processing of X-ray diffraction data collected in oscillation mode. In *Macromolecular Crystallography, Part A* (Carter, C. W., Jr & Sweet, R. M., eds), pp. 307–326, Academic Press, New York, NY.
51. Collaborative Computational Project No. 4. (1994). The CCP4 suite: programs for protein crystallography. *Acta Crystallogr., Sect. D: Biol. Crystallogr.* **50**, 760–763.
52. Brunger, A. T., Adams, P. D., Clore, G. M., DeLano, W. L., Gros, P., Grosse-Kunstleve, R. W. *et al.* (1998). Crystallography & NMR System: a new software suite for macromolecular structure determination. *Acta Crystallogr., Sect. D: Biol. Crystallogr.* **54**, 905–921.
53. Storoni, L. C., McCoy, A. J. & Read, R. J. (2004). Likelihood-enhanced fast rotation functions. *Acta Crystallogr., Sect. D: Biol. Crystallogr.* **60**, 432–438.
54. Emsley, P. & Cowtan, K. (2004). Coot: model-building tools for molecular graphics. *Acta Crystallogr., Sect. D: Biol. Crystallogr.* **60**, 2126–2132.